Journal of Molecular Graphics and Modelling 58 (2015) 10–15

Contents lists available at ScienceDirect

Journal of Molecular Graphics and Modelling

journal homepage: www.elsevier.com/locate/JMGM

Short communication

A dimension map for molecular aggregates

Cuiying Jian, Tian Tang*, Subir Bhattacharjee[1]

Department of Mechanical Engineering, University of Alberta, Edmonton, AB T6G 2G8, Canada

ARTICLE INFO

Article history:
Accepted 22 February 2015
Available online 2 March 2015

Keywords:
Gyradius ratios
Dimension map
Molecular aggregates
Aggregation manner
Solubility
Aggregation mechanism

ABSTRACT

A pair of gyradius ratios, defined from the principal radii of gyration, are used to generate a dimension map that describes the geometry of molecular aggregates in water and in organic solvents. Molecular dynamics simulations were performed on the aggregation of representative biomolecules and polyaromatic compounds to demonstrate application of the dimension map. It was shown that molecular aggregate data on the dimension map were bounded by two boundary curves, and that the map could be separated into three regions representing three groups of structures: one-dimensional rod-like structures; two-dimensional planar structures or short-cylinder-like structures; and three-dimensional sphere-like structures. Examining the location of the aggregates on the dimension map and how the location changes with solvent type and solute material parameter provides a simple yet effective way to infer the aggregation manner and to study solubility and mechanism of aggregation.

Aggregation of molecules is a universal phenomenon which occurs in many processes. For instance, proteins or peptides are associated together to form fibrils in a number of human diseases; phospholipid molecules in water can spontaneously aggregate into bilayer membranes; organic molecules possessing polyaromatic (PA) cores, such as perylene tetracarboxylic diimide, can assemble into semiconductors of nanobelt structures in solutions; heavy aromatics in crude oil known as asphaltenes aggregate during petroleum processing [1–5]. Depending on the aggregation mechanisms, various shapes can be formed, examples including spherical micelles or rod-like micelles [6–8]. These structures have been revealed by imaging techniques such as scanning electron microscopy, atomic force microscopy, transmission electron microscopy, circular dichroism, nuclear magnetic resonance, small-angle neutron scattering, as well as molecular dynamics (MD) simulations [4,6–11]. Many parameters have been used to define the shapes of various aggregates, such as radii of curvature employed in the work of Israelachvili et al. [12]. However, most of them are difficult to obtain numerically and/or experimentally, and hence, are not widely used. On the other hand, a consistent and generalized method quantifying dimension characteristics will facilitate direct comparison among different observations, which helps not only to track the morphology variations of molecular aggregates but also gain insight into the aggregation manner and driving forces. In this communication, we introduce a dimension map based on a pair of unitless quantities, defined from the ratios between the principal radii of gyration of the aggregated structures, as a simple way to quantify their dimension characteristics. Applications of the dimension map are demonstrated using aggregates formed by biomolecules as well as PA compounds in water and organic solvents, obtained from MD simulations. Its potential use in experimental studies, such as microscopic analysis of molecular aggregates, is discussed.

Seven different compounds selected from the categories of peptides, lipids and PA compounds were simulated using MD. Their chemical structures are shown in Fig. 1. Tetra-peptide (TYR-TYR-TYR-TYR, TYR-4; Fig. 1a) was selected as a representative for peptide. Dodecylphosphocholine (DPC; Fig. 1b) and dipalmitoylphosphatidylcholine (DPPC; Fig. 1c) were chosen as representatives for single- and double-chained lipids, respectively. Peptides and lipids are known to aggregate in aqueous environment [1,2]; hence they were simulated in water. PA compounds are often used as surrogates in petroleum engineering for probing the aggregation behaviors of asphaltenes [13], which are defined as toluene soluble but *n*-heptane insoluble heavy aromatic compounds [14–17]. Four PA models, developed from Viloanthrone-78 [18,19], were employed in the MD simulations. These four models have the same PA core but differ by the length of their aliphatic side chains. Based on the number of interconnected aliphatic hydrocarbons on each chain, the four models are respectively referred to as VO-4C (Fig. 1d), VO-8C (Fig. 1e), VO-12C (Fig. 1f) and VO-16C (Fig. 1g). Three solvents (water, toluene and *n*-heptane) were

* Corresponding author. Tel.: +1 780 492 5467; fax: +1 780 492 2200.
E-mail address: tian.tang@ualberta.ca (T. Tang).
[1] Present address: Water Planet Engineering, 721D, South Glasgow Avenue, Inglewood, CA 90301, United States. Tel.: +1 424 331 7702.

http://dx.doi.org/10.1016/j.jmgm.2015.02.003
1093-3263/

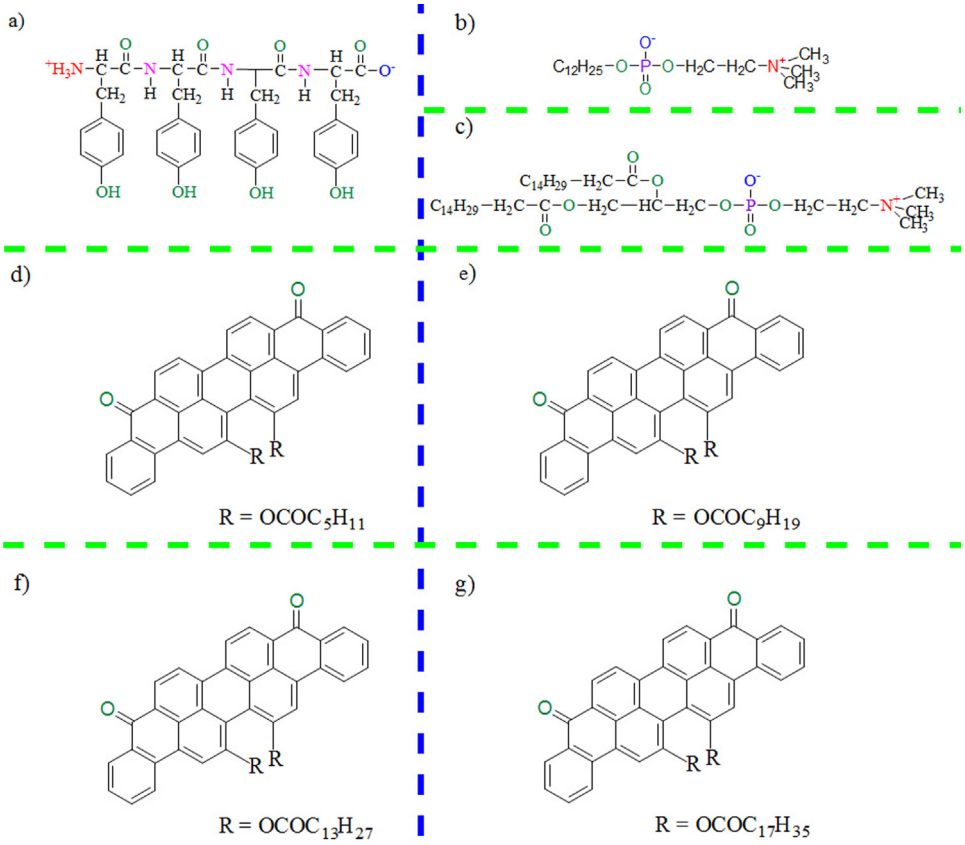

Fig. 1. Molecular structures employed in this study: (a) TYR-4, (b) DPC, (c) DPPC, (d) VO-4C, (e) VO-8C, (f) VO-12C and (g) VO-16C.

used in their MD simulations. In total, 15 systems were studied, all of which were simulated using GROMACS 4.0.7 [20–23] based on the GROMOS96 force field parameter set 53A6 [24]. Each system was subjected to an NPT simulation of length varying from 30 to 180 ns. Details on the MD simulations are available in the Supporting Information, Section S1.

Fig. 2 shows snapshots of selected aggregated structures obtained at the equilibrium stage of the simulations. The achievement of dynamic equilibrium is demonstrated in the Supporting Information, Section S2. It can be clearly seen that these aggregates exhibit different geometries. For example, the stacked PA cores of VO-8C in *n*-heptane (Fig. 2f) form a nearly one-dimensional structure not observed in other subfigures. In order to quantitatively describe the dimension of each aggregate, we define a pair of unitless quantities called gyradius ratios, based on the principal radii of gyration (gyradii) [25,26]. Specifically, for an aggregate we denote the three principal axes that pass through its center of mass as x, y, z and the three principal mass moments of inertia as I_{xx}, I_{yy}, I_{zz}. The detailed procedure of determining the principal mass moments of inertia and principal axes are available in the Supporting Information, Section S3. The principal radii of gyration are defined by [27–29]:

$$R_x = \left(\frac{I_{xx}}{\sum_i m_i}\right)^{0.5} = \left(\frac{\sum_i m_i(y_i^2 + z_i^2)}{\sum_i m_i}\right)^{0.5} \quad (1)$$

$$R_y = \left(\frac{I_{yy}}{\sum_i m_i}\right)^{0.5} = \left(\frac{\sum_i m_i(x_i^2 + z_i^2)}{\sum_i m_i}\right)^{0.5} \quad (2)$$

$$R_z = \left(\frac{I_{zz}}{\sum_i m_i}\right)^{0.5} = \left(\frac{\sum_i m_i(x_i^2 + y_i^2)}{\sum_i m_i}\right)^{0.5} \quad (3)$$

where m_i and (x_i, y_i, z_i) are respectively the mass and coordinates for atom i and the summations are over all atoms in a given aggregate. One can always denote R_0 as the minimum of $\{R_x, R_y, R_z\}$, R_2 as the maximum of $\{R_x, R_y, R_z\}$, and R_1 as the intermediate value among $\{R_x, R_y, R_z\}$. The gyradius ratios r_1 and r_2 are then defined as:

$$r_1 = \frac{R_1}{R_0}, \quad r_2 = \frac{R_2}{R_0} \quad (4)$$

Clearly $r_1 \le r_2$. Furthermore, it can be shown that for any structure, $1 \le r_1 \le r_2 \le \sqrt{1 + r_1^2}$ (see Supporting Information, Section S4). Therefore, if we generate a dimension map with r_1 and r_2 being the horizontal and vertical axes respectively (Fig. 3), any one aggregate will correspond to a point on this map, and all the points will be bounded by two curves of $r_2 = r_1$ and $r_2 = \sqrt{1 + r_1^2}$. These two curves are plotted as black dashed lines in Fig. 3. As r_1 increases, the two curves will approach each other, and eventually become indistinguishable when $r_1 \gg 1$. We now examine the gyradius ratios of the aggregates formed in our MD simulations and their locations on this dimension map.

Examples of final aggregated structures formed by TYR-4 and DPC are shown in Fig. 2a and b, respectively. In each system, the molecules formed 2 aggregates (one shown in Fig. 2) and each aggregate is more or less isotropic, with approximately equal dimensions in all directions. The gyradius ratios (r_1, r_2) for these aggregates are depicted in Fig. 3 as purple diamonds and purple plus signs, respectively for TYR-4 and DPC. All data points are located in the lower left region of the dimension map and near the boundary line of $r_2 = r_1$. This corresponds to a geometry which has approximately equal principal axes and resembles a three-dimensional sphere-like structure. In the system of DPPC, on the other hand, a single bilayer structure was formed (Fig. 2c) where the tail groups (colored cyan) are sandwiched between the head groups (colored

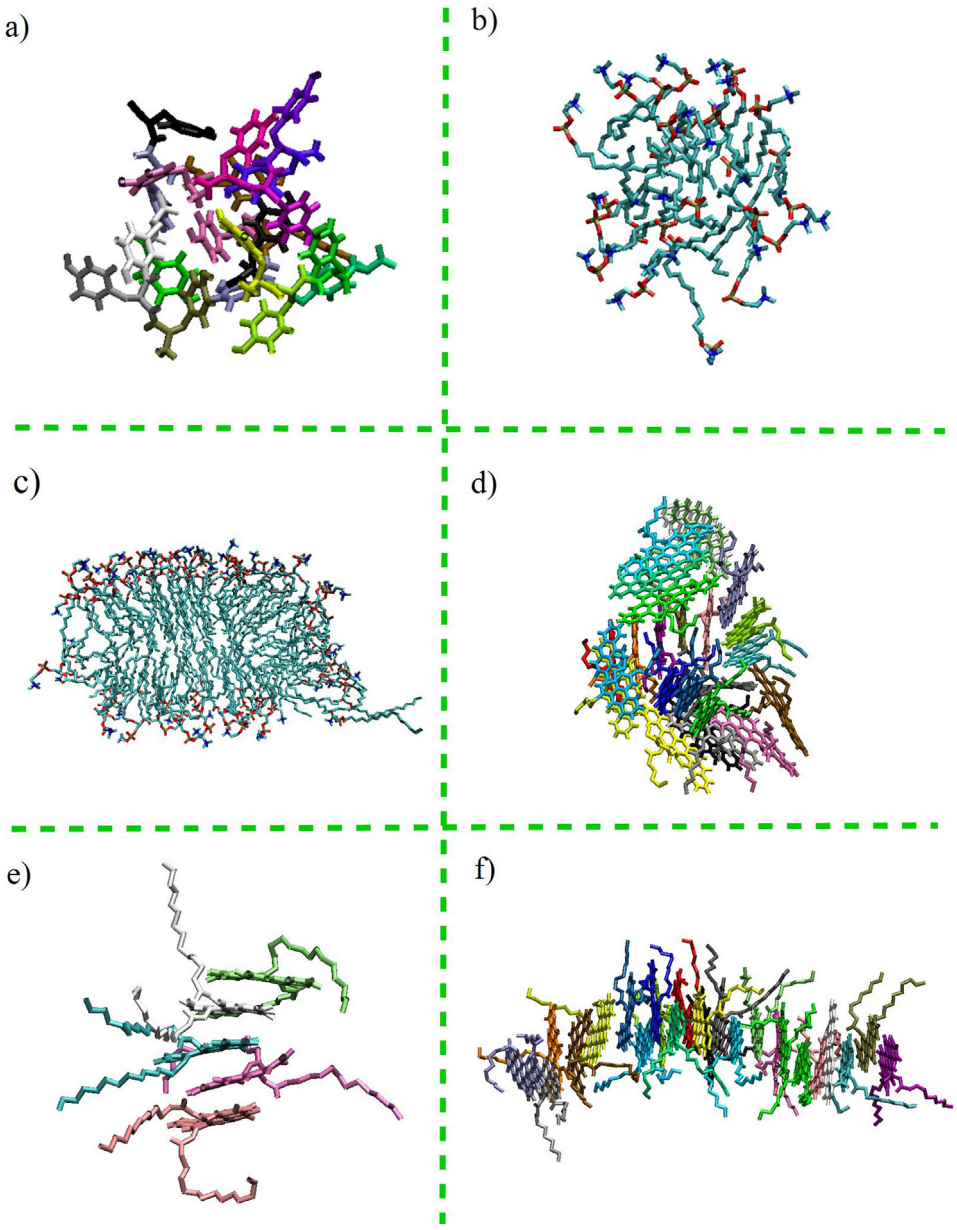

Fig. 2. Snapshots of the final aggregates formed by: (a) TYR-4 in water, (b) DPC in water, (c) DPPC in water, (d) VO-4C in water, (e) VO-12C in toluene and (f) VO-8C in *n*-heptane. In all subfigures, solvent molecules are removed for clarity.

red and blue). The point for the corresponding gyradius ratios, depicted by purple filled circle in Fig. 3, is well distinguished from those of DPC aggregates (see more discussion on DPPC in Supporting Information, Section S5) and lies in a region where some data of the PA compounds are located, as discussed below.

Selected final aggregated structures for PA compounds in water, toluene and *n*-heptane are shown in Fig. 2d–f, respectively. Inside each system, more than one aggregate may be formed. Only one aggregate is shown in Fig. 2 as a representative structure, whereas in Fig. 3 all the aggregates formed are represented by individual symbols. Because each PA molecule consists of a PA planar region, the PA cores from two molecules can stack in a parallel fashion due to the $\pi - \pi$ interaction between them [30–32]. For PA molecules in water (Fig. 2d), while some PA core stacking is observed, most molecules are simply entangled together, without a clearly preferred orientation in the aggregate. The final structure shares some similarities with the aggregates formed by TYR-4 and DPC and is close to a three-dimensional sphere. This is reflected in Fig. 3 where almost all the data for PA aggregates in water are located in the lower left region of the dimension map and near the boundary line of $r_2 = r_1$. Unlike in water, for PA molecules in *n*-heptane (Fig. 2f), the majority of the aggregates consist of many molecules with their PA cores parallel stacked in interior and side chains solvated in exterior. The parallel stacking persists for a long distance, much larger than the length scale of each PA molecule. As a result, a nearly one-dimensional rod-like structure is formed. Accordingly in Fig. 3, the gyradius ratios for PA aggregates in *n*-heptane are mostly located in the upper right region of the dimension map. In this region, the difference between the two boundary curves becomes smaller; r_1 and r_2 are of similar magnitude and are much greater than one, which is exactly the characteristic of a one-dimensional rod-like structure. The location of the PA aggregates in toluene on the dimension map is more puzzling. From Fig. 2e, the aggregate clearly exhibits different characteristics compared with Fig. 2d in water and Fig. 2f in *n*-heptane: unlike the random entanglement in water, the PA cores form ordered one-on-one stacking in toluene, but compared with in

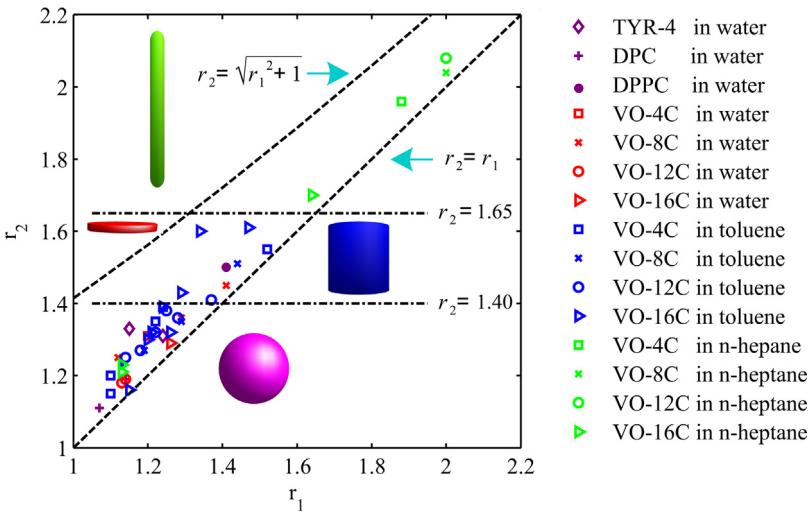

Fig. 3. Dimension map for the aggregates formed in the MD simulations.

n-heptane the parallel stacking persists for a much shorter distance. Similar structural arrangements as seen in Fig. 2e were observed for all aggregates formed by PA compounds in toluene. On the other hand, their corresponding gyradius ratios on the dimension map are distributed in a range: some located in the lower left region, while others located in the middle region with moderate r_1 and r_2 values.

To further investigate this, we first divide the dimension map into three regions, each representing a particular group of structures:

(I) $r_1 \geq 1.65$, which represents one-dimensional rod-like structures (length of rod much larger than the diameter).
(II) $1.40 < r_2 < 1.65$, which represents short-cylinder-like structures (when the data are near the lower boundary of $r_2 = r_1$, length of rod comparable to the diameter) or two-dimensional planar structures (when the data are near the upper boundary of $r_2 = \sqrt{1 + r_1^2}$).
(III) $r_2 \leq 1.40$, which represents three-dimensional sphere-like structures.

The boundary lines of $r_2 = 1.40$ and $r_2 = 1.65$ were chosen based on the natural gaps found on the dimension map. Using PA compounds as an example, for each simulated system, we calculated the percentages of molecules that participated in each type of structure and summarized them in Table 1. For instance, for VO-16C in *n*-heptane, the formed type (I) aggregate involves 16 molecules, resulting in a percentage of 16/24 = 66.67%. It can be clearly seen that in water, sphere-like structures dominate, with 100% for VO-4C, VO-12C and VO-16C, and near 80% for VO-8C. In *n*-heptane, rod-like structures are of the largest percentage, with 100% for VO-4C, VO-8C and VO-12C, and close to 70% for VO-16C. In toluene, both type (II) and type (III) structures are found for all the four types of PA molecular models.

With the above calculation, we now re-examine the location of the PA aggregates in toluene on the dimension map. While type (III) aggregates are dominant for PA aggregates in both toluene and water, compared with in water where type (II) aggregates are only formed by VO-8C molecules, all the four PA compounds can form type (II) structures in toluene. In fact, if individual dimension maps are generated for VO-4C, VO-12C and VO-16C (see Supporting Information, Fig. S2), the data associated with different solvents (water, toluene and *n*-heptane) can be easily distinguished on each map. This allows us to infer that the molecular arrangements in the PA aggregates should be different in the two different solvents (water and toluene). In addition, while for PA compounds with shorter side chains, their type (II) aggregates in toluene are all located close to the $r_2 = r_1$ curve, type (II) aggregates formed by VO-16C in toluene have shown the trend of moving toward the $r_2 = \sqrt{1 + r_1^2}$ boundary, which represents planar structures. If the PA molecules in toluene tend to form disordered aggregates like those in water through random entanglement of PA cores and side chains, such planar structures cannot be formed. Therefore one may suspect that, regardless of the side chain length, an ordered stacking structure of PA cores is formed for each aggregate in toluene with the side chains fully solvated. The stacking of the PA cores tends to promote the formation of a cylindrical structure, while the solvation and flexibility of side chains can make the overall geometry of an aggregate close to a sphere, if the stacking does not persist for a long distance as in *n*-heptane. These two competing factors are the reason why both type (II) and type (III) structures are present in toluene. In addition, if the side chain length is so long that it exceeds the range of stacking in the aggregates, the dimension in the plane perpendicular to the stacking direction will be large enough to make the aggregate resemble a planar structure; such a trend is observed for VO-16C. The aggregation manner inferred from the dimension map is consistent with previous visual observation in Fig. 2, and can be further verified by plotting the gyradius ratios generated using the PA cores on the same dimension map (see the Supporting Information, Section S7).

What structure will be formed when certain molecules aggregate in a given solvent is related to the solubility of the molecules. For example, the PA aggregates in toluene (type (III) and type (II) structures) differ from those in *n*-heptane (mainly type (I) structure) by the range of stacking. The smaller distance over which stacking persists in toluene indicates better solubility of PA compounds in toluene, which is consistent with the fact for the same total number (24) of PA molecules simulated, toluene gives rise to the most number of aggregates (number of data points on the dimension map; see Fig. 3) among the three solvents, and consistent with the definition of asphaltenes these PA compounds represent [14–17]. The structure of the aggregates is ultimately determined by the interaction between solutes, as well as the interaction between solute and solvent. Quantification and comparison of dimensional characteristics of the aggregates based on the dimension map helps us understand such interactions and hence the mechanisms of aggregation. For example, DPC molecules aggregate in water due to the hydrophobic interaction among them.

Table 1
Percentage of molecules that participated in each type of aggregated structures of PA compounds in different solvents.

Criteria	$r_2 \geq 1.65$ (type I)			$1.40 < r_2 < 1.65$ (type II)			$r_2 \leq 1.40$ (type III)		
Solvent	Water	Toluene	*n*-Heptane	Water	Toluene	*n*-Heptane	Water	Toluene	*n*-Heptane
VO-4C			100%		29.17%		100%	70.83%	
VO-8C			100%	20.83%	43.48%		79.17%	56.52%	
VO-12C			100%		30.43%		100%	69.57%	
VO-16C			66.77%		25%		100%	75%	33.33%

The hydrophobic tails (depicted by cyan colors in Fig. 2b) tend to associate together to minimize their contact with water while exposing the hydrophilic head groups (depicted by red and blue colors in Fig. 2b) to water [33]. The sphere-like structure formed from the aggregation is consistent with such interaction. It is well-known that the shape of the aggregates formed by lipids depends on their molecular structure [33], while single-chained lipids tend to form spherical micelles, double-chained lipids tend to form bilayer structures due to their large hydrocarbon volume. This is evident from the simulation and dimension map. For PA compounds in toluene, the progression of aggregates from type (III) into type (II) and the trend of forming planar structures by VO-16C has allowed us to conclude that ordered short-ranged stacking is formed in toluene, which suggests that the main driving force for aggregation of PA compounds in toluene is the $\pi - \pi$ stacking between PA cores [34]. In comparison, the much larger range of stacking observed for PA compounds in *n*-heptane suggests that much greater solvent–solute attraction exists for the same PA molecules in toluene [34,35]. Almost all the aggregates formed by PA compounds in water are sphere-like. This indicates that $\pi - \pi$ stacking between PA cores is not the only mechanism driving aggregation in water. In fact, the hydrophobic associations among the aliphatic side chains played an important role in causing the aggregation, prohibiting the formation of ordered stacking structures [18]. Particularly, for VO-8C which has intermediate side-chain length, the decreased $\pi - \pi$ stacking and the insufficient hydrophobic association has led to the smallest percentage of sphere-like structure in water among all the PA compounds. Additionally, despite the very different size and molecular structure TYR-4, DPC and PA molecules have, their aggregates in water are located in the same region on the dimension map, suggesting that hydrophobic interaction as a common critical driving force in their aggregation.

Apart from its applications in MD studies, the dimension map proposed here can also be used for experimental structure characterization. For instance, in determining the size and shape of gas phase molecules, the three principal mass moments of inertial for a molecule can be obtained by spectroscopic measurements in the microwave region [36], and according to their relationships, molecular shapes have been roughly classified into linear, symmetric top, spherical top and asymmetric top categories [37]. Since the gyradius ratios can be directly calculated from the principal mass moments of inertia, these molecules can be easily located onto the dimension map, which helps to quantitatively compare molecular structures and further understand the structure–function relationship. Mathematically, gyradius ratios introduced in this work share some similarities with the asphericity defined for studying the shape of polymers [38], which is also derived based on the principal moments of inertia. On the other hand, asphericity only describes the deviation of a geometry shape from spherical symmetry, while our dimension map further provides a more complete way to directly differentiate geometries. More importantly, adopting image analysis method described in the work by Maurstad et al. [39], principal moments of inertia for molecular aggregates can be obtained from atomic force microscopy topographs. Hence, gyradius ratios can be easily calculated to generate a comprehensive dimension map, where the direct morphology comparison between numerical simulations and experiments can be made to shed lights on understanding the aggregation process. Furthermore, accurate knowledge of the aggregates' geometries and hence the associated molecular aggregation manner can help us infer the chemical structures of aggregated molecules. For instance, in the petroleum field atomic structures of large asphalt compounds are often under debate [5]. By measuring the geometries of their aggregates in different solvents and locating them on the dimension map, their solubility behavior, potential aggregation driving forces and interaction with different solvents can be determined, which can provide new insight into their chemical structures.

In conclusion, we introduce a simple but effective way to quantify the geometry of molecular aggregates often seen in biology as well as in industrial complex fluids. A dimension map is generated based on a pair of unitless numbers named gyradius ratios. Aggregated structures can be categorized into different groups according to the locations of their gyradius ratios on the dimension map. Examining the location of the aggregates on the dimension map and how the location changes with solvent type and solute material parameter can help us infer the aggregation manner and understand mechanisms driving aggregation in a given solvent, and it can be applied to both simulations and experiments. It should be noted that we focus on providing quantification for structures resulting from molecular aggregation of soft condensed matter, which typically do not have unusual geometries such as sharp corners. Description of all geometries (particularly crystalline structures) that can exist mathematically is out of the scope of this work.

Acknowledgements

We acknowledge the computing resources and technical support from Western Canada Research Grid (WestGrid). Financial support for this research from Natural Sciences and Engineering Research Council (NSERC) of Canada, Canada Foundation for Innovation, and Alberta Innovates-Technology Futures (AI-TF) is gratefully acknowledged. Cuiying Jian acknowledges financial support from University of Alberta Doctoral Recruitment Scholarship, the Jacob H Masliyah Graduate Award in Oil Sands Engineering and Alberta Innovates Graduate Student Scholarship.

Appendix A. Supplementary data

Supplementary data associated with this article can be found, in the online version, at http://dx.doi.org/10.1016/j.jmgm.2015.02.003.

References

[1] C. Wu, H. Lei, Y. Duan, J. Am. Chem. Soc. 127 (2005) 13530–13537.
[2] S.J. Marrink, E. Lindahl, O. Edholm, A.E. Mark, J. Am. Chem. Soc. 123 (2001) 8638–8639.
[3] K. Balakrishnan, A. Datar, R. Oitker, H. Chen, J. Zuo, L. Zang, J. Am. Chem. Soc. 127 (2005) 10496–10497.
[4] K. Balakrishnan, A. Datar, T. Naddo, J. Huang, R. Oitker, M. Yen, J. Zhao, L. Zang, J. Am. Chem. Soc. 128 (2006) 7390–7398.
[5] J.G. Speight, The Chemistry and Technology of Petroleum, fourth ed., CRC Press, Boca Raton, 2006.
[6] A.V. Sangwai, R. Sureshkumar, Langmuir 27 (2011) 6628–6638.

[7] M. Velinova, D. Sengupta, A.V. Tadjer, S. Marrink, Langmuir 27 (2011) 14071–14077.
[8] Z. Liu, Y. Shang, J. Feng, C. Peng, H. Liu, Y. Hu, J. Phys. Chem. B 116 (2012) 5516–5526.
[9] S. Benjwal, S. Verma, K. Röhm, O. Gursky, Protein Sci. 15 (2006) 635–639.
[10] M. Törnblom, U. Henriksson, J. Phys. Chem. B 101 (1997) 6028–6035.
[11] G. Porte, J. Marignan, P. Bassereau, R. May, J. Phys. 49 (1988) 511–519.
[12] J.N. Israelachvili, D.J. Mitchell, B.W. Ninham, J. Chem. Soc., Faraday Trans. 2 72 (1976) 1525–1568.
[13] B. Breure, D. Subramanian, J. Leys, C.J. Peters, M.A. Anisimov, Energy Fuels 27 (2012) 172–176.
[14] J.G. Speight, R.B. Long, T.D. Trowbridge, Fuel 63 (1984) 616–620.
[15] H. Groenzin, O.C. Mullins, J. Phys. Chem. A 103 (1999) 11237–11245.
[16] H.W. Yarranton, H. Alboudwarej, R. Jakher, Ind. Eng. Chem. Res. 39 (2000) 2916–2924.
[17] T.F. Headen, E.S. Boek, N.T. Skipper, Energy Fuels 23 (2009) 1220–1229.
[18] C. Jian, T. Tang, S. Bhattacharjee, Energy Fuels 27 (2013) 2057–2067.
[19] A.B. Andrews, A. McClelland, O. Korkeila, A. Demidov, A. Krummel, O.C. Mullins, Z. Chen, Langmuir 27 (2011) 6049–6058.
[20] B. Hess, C. Kutzner, D. Van Der Spoel, E. Lindahl, J. Chem. Theory Comput. 4 (2008) 435–447.
[21] D. Van Der Spoel, E. Lindahl, B. Hess, G. Groenhof, A.E. Mark, H.J. Berendsen, J. Comput. Chem. 26 (2005) 1701–1718.
[22] E. Lindahl, B. Hess, D. Van Der Spoel, Mol. Model. 7 (2001) 306–317.
[23] H.J. Berendsen, D. van der Spoel, R. van Drunen, Comput. Phys. Commun. 91 (1995) 43–56.
[24] C. Oostenbrink, A. Villa, A.E. Mark, W.F. Van Gunsteren, J. Comput. Chem. 25 (2004) 1656–1676.
[25] P. Rigo, J. Hydrosci. Hydraul. Eng. 10 (1992) 27–36.
[26] J.H. Allen III, Mechanics of Materials for Dummies, Wiley Publishing Inc., Hoboken, 2011.
[27] J.L. Meriam, L.G. Kraige, Engineering Mechanics: Dynamics, sixth ed., John Wiley & Sons Inc., 2007.
[28] J. Wittenburg, Dynamics of Multibody Systems, Springer, Berlin, 2007.
[29] A. Pytel, J. Kiusalaas, Engineering Mechanics: Dynamics, third ed., Cengage Learning, Stamford, 2010.
[30] J.P. Dickie, T.F. Yen, Anal. Chem. 39 (1967) 1847–1852.
[31] T. Yen, Energy Sources 1 (1974) 447–463.
[32] J. Murgich, Pet. Sci. Technol. 20 (2002) 983–997.
[33] J.N. Israelachvili, Intermolecular and Surface Forces, third ed., Academic press, San Diego, CA, 2011.
[34] C. Jian, T. Tang, S. Bhattacharjee, Energy Fuels 28 (2014) 3604–3613.
[35] C. Jian, T. Tang, J. Phys. Chem. B 118 (2014) 12772–12780.
[36] J. Kraitchman, Am. J. Phys. 21 (1953) 17–25.
[37] M.C. Gupta, Atomic and Molecular Spectroscopy, New Age International (P) Ltd., New Delhi, 2007.
[38] J. Rudnick, G. Gaspari, J. Phys. A: Math. Gen. 19 (1986) L191–L193.
[39] G. Maurstad, S. Danielsen, B.T. Stokke, J. Phys. Chem. B 107 (2003) 8172–8180.